ENHANCED MASS CONSERVATION IN LEAST-SQUARES METHODS FOR NAVIER-STOKES EQUATIONS[*]

J. J. HEYS[†], E. LEE[‡], T. A. MANTEUFFEL , S. F. MCCORMICK , AND J. W. RUGE[§]

Abstract. There are many applications of the least-squares finite element method for the numerical solution of partial differential equations because of a number of benefits that the least-squares method has. However, one of most well-known drawbacks of the least-squares finite element method is the lack of exact discrete mass conservation, in some contexts, due to the fact that least-squares method minimizes the continuity equation in L^2 norm. In this paper, we explore the reason of the mass loss and provide new approaches to retain the mass even in severely under-resolved grid.

Key words. Navier-Stokes equations, mass conservation, least-squares finite element method

1. Introduction. The finite element method based on first-order system least-squares (FOSLS) formulation has been used in a wide variety of applications [3], [4], [5], [6], [11]. We are interested, here, in least-squares finite element methods for Stokes and Navier-Stokes equations. The advantages of FOSLS formulation include: many properties of the continuous space are naturally inherited by the discrete finite-dimensional subspace; weak formulations associated with the minimization problems are, in general, coercive; the resulting algebraic problems are symmetric and positive definite; the FOSLS functional provides an excellent local a posteriori error measure; and the choice of discretization spaces is not restricted [1], [2], [3], [4], [7], [12]. On the other hand, least-squares methods for Stokes and Navier-Stokes equations lack an exact sense of discrete mass conservation. More precisely, least-squares methods do not naturally constrain the velocities to exactly satisfy any form of the mass conservation equations on discrete volumes as Galerkin and finite volume methods typically do. Instead, these methods merely strike a balance between the L^2 errors in each equation, with no special attention to the one that expresses mass conservation. Conservation error generally tends to vanish as the resolution or approximation order increases, but some applications require a level of discrete conservation that substantially exceeds the overall accuracy obtained by the discretization. In particular, for problems in which the domain is long and thin and only velocity boundary conditions are prescribed on all but a relatively small portion of the boundary, the use of low-order finite element spaces with a relatively coarse grid without further mitigation can result in severe mass loss. This deficiency can be overcome in two-dimensional problems by using higher-order finite element spaces, as the results in [15] show. However, in three dimensions, further measures may be necessary, which is the focus of this paper.

In [9], mass conservation was improved by introducing newly defined variables and corresponding boundary conditions. Here, we instead suggest more fundamental ways of achieving improved mass conservation. We first identify a cause of the loss of mass in the least-squares finite element method in three-dimensional problems. In section 3, we show that boundary conditions near edges parallel to the flow contribute to mass-loss, even when high-order finite elements are employed. In section 3.1, a

[†]Chemical Engineering Department, Arizona State University, Tempe, AZ 85287 (`heys@asu.edu`)

[‡]School of Computational Science, Florida State University, Tallahassee, FL 32306 (`eunjung@scs.fsu.edu`)

[§]Department of Applied Mathematics, University of Colorado at Boulder, Boulder, CO 80309 (`tmanteuf@colorado.edu,stevem@colorado.edu, John.Ruge@colorado.edu`)

modification of the way in which boundary conditions are applied is proposed that greatly enhances mass conservation. In section 3.2, a weighted boundary functional is employed near these edges that yields a similar restoration of mass conservation.

Another technique, described in section 3.3, involves the use of both first-order system least-squares (FOSLS) [7] and first-order system LL* (FOSLL*) [8] methods. FOSLS is an approach that rewrites the original equations as a first-order system to which a least-squares minimization principle is applied. The usual aim of FOSLS is to produce a functional that is equivalent to the square of a product H^1 norm. FOSLL* also rewrites the original equations as a first-order system, but then formulates an H^1-equivalent minimization principle (in the linear case) by introducing the dual variables via the adjoint of the associated first-order operator. In this paper, we combine these two methods. First, we solve a linear system with FOSLS and add a correction from FOSLL* to get an enhanced approximation. FOSLS provides an approximation in a current least-squares finite dimensional space and FOSLL* provides a correction from a different finite dimensional space to recover the mass loss (see the details in subsection 3.3). This framework fits well for nonlinear systems because solving for a correction with FOSLL* is no more costly than one linearization step in a Newton iteration. To our knowledge, this is the first attempt to combine FOSLS and FOSLL* in this way. This paper focuses on improving the approximation in terms of mass conservation for Stokes and Navier-Stokes using FOSLS/FOSLL* approach.

Our model problem is introduced in section 2. In section 3, several approaches for improving mass conserving least-squares methods are developed. We then apply these approaches to the Navier-Stokes equations in section 4.

2. Model problem. Consider the steady state Navier-Stokes equations:

$$\begin{aligned} -Re\mathbf{u} \cdot \nabla\mathbf{u} - \nabla p + \Delta\mathbf{u} &= \mathbf{0} \quad \text{in } \Omega, \\ \nabla \cdot \mathbf{u} &= 0 \quad \text{in } \Omega, \\ \mathbf{u} &= \mathbf{g} \quad \text{on } \partial\Omega, \end{aligned} \quad (2.1)$$

where Re is the Reynolds number and p is the pressure normalized by viscosity. The situation that seems to produce the most dramatic loss of mass is a long thin domain with velocity boundary conditions, and so we focus on these. Throughout this paper, the vector valued variables are in boldface characters and the scalar valued variables are in roman characters, respectively.

We recast (2.1) as two well-known equivalent first-order systems, called *velocity/velocity-gradient/pressure* and *velocity/vorticity/pressure* formulations [4]. By introducing a new dependent variable, $\mathbf{U} = \nabla\mathbf{u}$, the equivalent first-order *velocity/velocity-gradient/pressure* formulation is given by

$$\begin{aligned} \mathbf{U} - \nabla\mathbf{u} &= \mathbf{0} \quad \text{in } \Omega, \\ \nabla \cdot \mathbf{u} &= 0 \quad \text{in } \Omega, \\ -Re\mathbf{u} \cdot \mathbf{U} - \nabla p + \nabla \cdot \mathbf{U} &= \mathbf{0} \quad \text{in } \Omega, \\ \nabla \times \mathbf{U} &= \mathbf{0} \quad \text{in } \Omega, \\ \nabla(tr\mathbf{U}) &= \mathbf{0} \quad \text{in } \Omega, \\ \mathbf{u} &= \mathbf{g} \quad \text{on } \partial\Omega, \\ \mathbf{n} \times \mathbf{U} &= \mathbf{G} \quad \text{on } \partial\Omega, \end{aligned} \quad (2.2)$$

where $tr\mathbf{U}$ represents the trace of $\mathbf{U}$. The boundary condition, $\mathbf{u} = \mathbf{g}$, yields the condition $\mathbf{n} \times \mathbf{U} = \mathbf{G}$. In system (2.2), the fourth and fifth equations are auxiliary equations induced from the first and the second equations, respectively. System (2.2)

is overdetermined, but consistent (see [1] for details). For all the numerical tests in this paper, we enforce the constraint $tr\mathbf{U} = 0$ by eliminating one of the dependent variables, that is, by setting $U_{33} = -(U_{11} + U_{22})$.

Using the vorticity field, $\mathbf{w} = \nabla \times \mathbf{u}$, we obtain the *velocity/vorticity/pressure* formulation:

$$
\begin{aligned}
\nabla \times \mathbf{u} + \nabla\alpha - \mathbf{w} &= \mathbf{0} && \text{in } \Omega, \\
\nabla \cdot \mathbf{u} &= 0 && \text{in } \Omega, \\
-Re\mathbf{u} \times \mathbf{w} + \nabla P + \nabla \times \mathbf{w} &= \mathbf{0} && \text{in } \Omega, \\
\nabla \cdot \mathbf{w} &= 0 && \text{in } \Omega, \\
\mathbf{u} &= \mathbf{g} && \text{on } \partial\Omega, \\
\alpha &= 0 && \text{on } \partial\Omega, \\
\mathbf{n} \cdot \mathbf{w} &= g && \text{on } \partial\Omega,
\end{aligned}
\tag{2.3}
$$

where α is a slack variable and $P = (Re/2)|\mathbf{u}|^2 + p$ denotes total pressure. The boundary condition, $\mathbf{u} = \mathbf{g}$, yields the condition $\mathbf{n} \cdot \mathbf{w} = g$.

From now on, we use velocity-gradient and vorticity for short to mean *velocity/velocity-gradient/pressure* and *velocity/vorticity/pressure*, respectively.

FOSLS rewrites these systems as minimization principles for the following respective velocity-gradient and vorticity functionals:

$$
\begin{aligned}
F(\mathbf{u}, \mathbf{U}, p : \mathbf{0}) = &\|\mathbf{U} - \nabla\mathbf{u}\|^2 + \|\nabla \cdot \mathbf{u}\|^2 \\
&+ \| - Re\mathbf{u} \cdot \mathbf{U} - \nabla p + \nabla \cdot \mathbf{U}\|^2 + \|\nabla \times \mathbf{U}\|^2 + \|\nabla(tr\mathbf{U})\|^2
\end{aligned}
\tag{2.4}
$$

and

$$
\begin{aligned}
G(\mathbf{u}, \alpha, \mathbf{w}, P : \mathbf{0}) = &\|\nabla \times \mathbf{u} + \nabla\alpha - \mathbf{w}\|^2 + \|\nabla \cdot \mathbf{u}\|^2 \\
&+ \| - Re\mathbf{u} \times \mathbf{w} + \nabla P + \nabla \times \mathbf{w}\|^2 + \|\nabla \cdot \mathbf{w}\|^2,
\end{aligned}
\tag{2.5}
$$

where $\|\cdot\|$ denotes the L^2-norm over domain Ω.

3. Mass conservation in Stokes equations. To simplify the discussion, we first consider Stokes equations, defined by $Re = 0$. The first test problem we examine is a long square tube with dimension $1 \times 1 \times 10$. We call the boundaries the inlet and outlet where $z = 0$ and $z = 10$, respectively, and walls otherwise. Along the walls, a no-slip boundary condition ($\mathbf{u} = \mathbf{0}$) is imposed. On then inlet and outlet, the boundary conditions are

$$
\mathbf{n} \times \mathbf{u} = \mathbf{0} \quad \text{and} \quad \mathbf{n} \cdot \mathbf{u} = x(1 - x)y(1 - y),
\tag{3.1}
$$

where $\mathbf{n}$ is the outward unit normal vector. On inlet and outlet, the flow profile is the parabola $x(1-x)y(1-y)$. The exact solution of this model problem does not maintain a parabolic profile in z cross-sections down the tube but, away from inlet/outlet, it does tend toward what is known as a developed steady flow that is independent of z. This is achieved with a profile, $u(x, y)$, satisfying $\Delta u(x, y) = C$ along the z-direction and the pressure, $p(x, y, z)$, satisfying $\nabla p = (0, 0, C)^t$. Here, C is chosen so that $\int_0^1 \int_0^1 u(x, y)dxdy = \frac{1}{36} = \int_0^1 \int_0^1 x(1 - x)y(1 - y)dxdy$, the cross-sectional flux.

In (2.2) and (2.3), letting $Re = 0$ implies $P = p$ and we then obtain the first-order systems of Stokes equations. The boundary conditions in (2.2) and (2.3) are valid for Stokes problem as well.
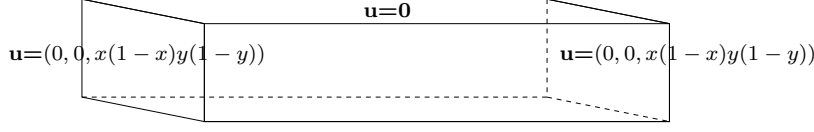
FIG. 3.1. *Domain*

The FOSLS velocity-gradient formulation uses the functional

$$F_S(\mathbf{u}, \mathbf{U}, p) = \|\mathbf{U} - \nabla\mathbf{u}\|^2 + \|\nabla \cdot \mathbf{u}\|^2$$
$$+ \|\nabla \cdot \mathbf{U} - \nabla p\|^2 + \|\nabla \times \mathbf{U}\|^2 + \|\nabla(tr\mathbf{U})\|^2 \qquad (3.2)$$

and the FOSLS vorticity formulation uses

$$G_S(\mathbf{u}, \alpha, \mathbf{w}, p) = \|\nabla\times\mathbf{u} + \nabla\alpha - \mathbf{w}\|^2 + \|\nabla \cdot \mathbf{u}\|^2 + \|\nabla\times\mathbf{w} + \nabla p\|^2 + \|\nabla \cdot \mathbf{w}\|^2. \qquad (3.3)$$

Under general H^2-regularity conditions, $F_S(\mathbf{u}, \mathbf{U}, p)$, with consistent boundary conditions on $\mathbf{u}$ and $\mathbf{n} \times \mathbf{U}$, is equivalent to the squared H^1-norm, $\|\mathbf{u}\|_1^2 + \|\mathbf{U}\|_1^2 + \|p\|_1^2$ [7]. Although (2.3) is perhaps the most widely used least-squares from of Stokes and Navier-Stokes equations [4], H^1-equivalence generally does not hold for $G_S(\mathbf{u}, \alpha, \mathbf{w}, p)$ with boundary conditions on $\mathbf{u}$ and $\mathbf{n} \cdot \mathbf{w}$ [2].

The software package FOSPACK [16] was used to construct the discrete systems and solve them by a conjugate gradient iteration preconditioned by algebraic multigrid (AMG) using W(1,1)-cycles. Table 3.1 shows the amount of mass loss in the approximate solution in the middle of the domain ($z = 5$), where the biggest loss occurs. Since we prescribe the outlet boundary conditions as inlet boundary conditions, mass loss is symmetric with respect to $z = 5$. Throughout this paper, the mass loss reported in the tables is the relative loss at $z = z_0$, where the biggest mass loss occurs, compared to the inlet flow rate:

$$\left(\int_{\Gamma_{in}} \mathbf{n} \cdot \mathbf{u} \, ds \; - \; \int_{\Gamma_{z_0}} \mathbf{n} \cdot \mathbf{u} \, ds \right) \Big/ \int_{\Gamma_{in}} \mathbf{n} \cdot \mathbf{u} \, ds,$$

where Γ_{in} is the inlet surface and $\int_{\Gamma_{z_0}} \mathbf{n} \cdot \mathbf{u} \, ds$ is the net flow across the plane $z = z_0$. The total flow rate into the domain is $1/36 \approx 2.778 \times 10^{-2}$. For the velocity-gradient formulation of the standard least-squares method, the flow rates in the middle of the domain ($z = 5$) are

$$h = 1/8, \; \text{Linear} : 8.099 \times 10^{-6} \; (99.9\% \text{ mass loss})$$
$$\longrightarrow \begin{cases} h = 1/16, \; \text{Linear} : 7.730 \times 10^{-4} \; (97.2\% \text{ mass loss}) \\ h = 1/8, \; \text{Quadratic} : 6.617 \times 10^{-3} \; (76.2\% \text{ mass loss}). \end{cases} \qquad (3.4)$$

As briefly mentioned in the introduction, using higher-order elements largely alleviates the mass loss in two dimension ([15]). In three dimensional space, increasing the order of elements is not as effective as in two dimension, but still provides better mass conservation than decreasing mesh size, as shown in (3.4). Thus, in this paper, we focus on using higher order elements. Also, we have changed mesh size, h, so that the same number of degrees of freedom are used for each type of finite element space, while we increase the order of the elements. However, the cost of solution is higher with higher-order elements because the matrices in the corresponding discrete system

	Velocity-Gradient		
	Linear $(h = 1/16)$	Quadratic $(h = 1/8)$	Quartic $(h = 1/4)$
mass loss	97.2%	76.2%	47%
functional value	1.109×10^{-2}	4.577×10^{-3}	2.284×10^{-3}
	Vorticity		
mass loss	99.96%	99.1%	92.5%
functional value	3.366×10^{-3}	1.275×10^{-3}	7.708×10^{-4}

TABLE 3.1

Mass loss and Functonal value: Square tube, Standard boundary normal vector

are more dense. In the vorticity formulation, the loss of mass is more severe. The functional value in the table below gives the values of F_S and G_S.

Since the velocity that is fully specified over all boundaries satisfies the global mass conservation constraint, only local mass conservation is violated. To explain one source of loss of mass, consider the boundary conditions on the velocity-gradient,

$$\mathbf{U} = \nabla \mathbf{u} = (\nabla u_1 \ \nabla u_2 \ \nabla u_3) = (U_1 \ U_2 \ U_3) = \begin{pmatrix} U_{11} & U_{21} & U_{31} \\ U_{12} & U_{22} & U_{32} \\ U_{13} & U_{23} & U_{33} \end{pmatrix}.$$

The no-slip boundary condition, $\mathbf{u} = \mathbf{0}$, on the walls implies $\mathbf{n} \times \mathbf{U} = \mathbf{0}$ on the walls. Together with the constraint $\nabla \cdot \mathbf{u} = tr\mathbf{U} = 0$, this yields $U_{i1} = U_{i3} = 0$, for $i = 1, 2, 3$, and $U_{22} = 0$ on top/bottom walls and $U_{i2} = U_{i3} = 0$, for $i = 1, 2, 3$, and $U_{11} = 0$ on left/right side walls. Now, consider the edge between the top and right walls. The conditions imply $U_{33} = 0$ on both walls, while $U_{31} = 0$ on the top and $U_{32} = 0$ on the right side. The equation for $\partial_z p$ is then

$$\nabla \cdot U_3 = \partial_x U_{31} + \partial_y U_{32} + \partial_z U_{33} = \partial_z p.$$

In developed flow, $\partial_z p = C$. While this is satisfied by the exact solution, it is difficult for functions in a finite element space to accommodate this condition. Near the corners, the result is that the pressure p is driven toward zero and remains near zero throughout the majority of the domain. The first line of graphs in figure 3.4 provides a profile of p from a velocity-gradient FOSLS formulation on a relatively coarse grid. Notice that the pressure drops quickly to zero. Small pressure corresponds to no flow, loss of mass, and a near zero solution in the center of the domain. It is important to note that this difficulty disappears as the grid is refined.

We confirm the above by observing the following example. Let the domain be a cylindrical tube, $\{(x, y) \mid x^2 + y^2 \leq 0.25\} \times [\, 0, 10 \,]$ (see fig 3.2), with the normal vector on the walls given by $\mathbf{n} = \left(x/\sqrt{x^2 + y^2}, y/\sqrt{x^2 + y^2}, 0 \right)^t$.

Walls : $x^2 + y^2 = 0.25$

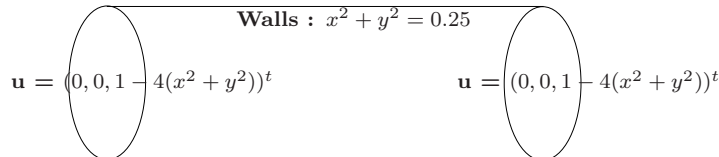$\mathbf{u} = (0, 0, 1 - 4(x^2 + y^2))^t \qquad \mathbf{u} = (0, 0, 1 - 4(x^2 + y^2))^t$

FIG. 3.2. *Mass loss: Cylindrical domain, Standard boundary conditions*

Simply using higher-order finite elements effectively diminishes mass loss (see table 3.2). Note, these computations employed isoparametric hexahedral elements.

	Velocity-Gradient		Vorticity	
	Linear($h = 1/20$)	Quad($1/10$)	Linear($1/20$)	Quad($1/10$)
mass loss	16%	0.02%	22.3%	0.03%
functional	2.284×10^{-1}	2.478×10^{-4}	2.092×10^{-1}	2.335×10^{-4}

TABLE 3.2

Mass loss: Cylindrical domain, Standard boundary normal vector

These observations motivate the definition of a smoothly defined normal vector. We can picture a domain with a corner rounded on the scale of the effective grid spacing. For such a corner, the normal vector, **n**, would change smoothly from one wall to the other. A similar approach would be to allow the normal vector, **n**, to be a continuous function of its position on the boundary.

3.1. Smoothly changing normal vector. To avoid overspecifying boundary conditions on the corners of the domain, we now define the normal vector as a continuous linear function of its position on the boundary. Consider the top right corner of the boundary. The normal vector is now defined by

$$\mathbf{n}(x, y, z) = \begin{cases} (0, 1, 0), & \text{when } x < 1 - \tau, \\ \left(\frac{x-1}{\tau} + 1, 1, 0\right) / \sqrt{\left(\frac{x-1}{\tau} + 1\right)^2 + 1}, & \text{when } 1 - \tau \le x \le 1, \end{cases}$$

on the top and

$$\mathbf{n}(x, y, z) = \begin{cases} \left(1, \frac{y-1}{\tau} + 1, 0\right) / \sqrt{1 + \left(\frac{y-1}{\tau} + 1\right)^2}, & \text{when } 1 - \tau \le y \le 1, \\ (1, 0, 0), & \text{when } y < 1 - \tau, \end{cases}$$

on the right wall near the corner for sufficiently small positive τ (see figure 3.3). The normal vectors on the other corners are defined in a similar manner. From numerical experiments, we have observed better results when when $\tau < h$, then when $\tau \ge h$ in terms of a mass conservation and functional value convergence. Thus, smoothing is employed only in the elements touching the corner. At the corners, the normal vector is defined as an averaged normal vector ([17]).

Computationally, the normal vector is only evaluated at quadrature points along the boundary. In all of the tests in this paper, τ was chosen sufficiently small so that only the normal vector at the corner was altered, as indicated in Figure 3.3. The mesh spacings used in this paper are relatively coarse, with $h = 1/16$ being the finest grid. In practice, we recommend only changing the normal vector in the corner regardless of the mesh spacing used. Because the normal vector is, in effect, only modified on an $O(h)$ portion of the boundary, the smoothly changing normal will have no effect on the eventual convergence of the discrete approximation to the exact solution.
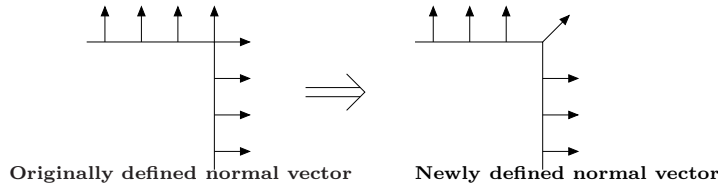

Originally defined normal vector   **Newly defined normal vector**

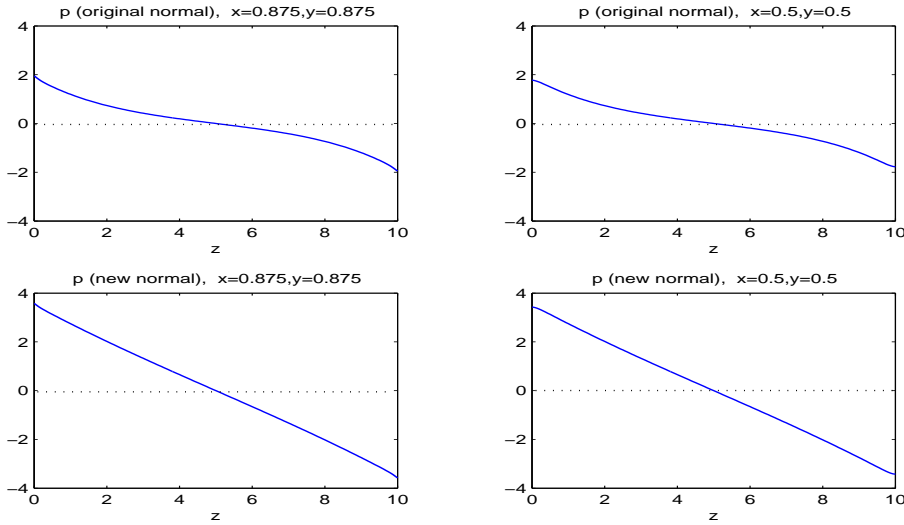FIG. 3.3. *Redefined normal vector*

As is apparent from table 3.3, simply redefining the normal vector on the four corners (along the edges in three dimensions) improves mass conservation for both

velocity-gradient and vorticity FOSLS formulations. Note that a mass loss of 2% is good considering that the grid, $h = 1/4$, is very coarse. We also observe an improved pressure near the corner and in the middle of domain from figure 3.4 (the second line).

Velocity-Gradient			
	Linear ($h = 1/16$)	Quadratic (1/8)	Quartic (1/4)
mass loss	92 %	17%	2%
functional value	8.592×10^{-3}	9.238×10^{-4}	1.252×10^{-4}
Vorticity			
mass loss	99.75%	63.2%	13.2%
functional value	2.897×10^{-3}	4.866×10^{-4}	8.138×10^{-5}

TABLE 3.3
Mass loss: Square tube, Smoothly changing normal vector

FIG. 3.4. *Pressure in velocity FOSLS (quadratic elements, $h = 1/8$)*

One advantage of using this newly defined normal vector is that it does not degrade multigrid performance while providing improved mass conservation (for example, AMG-convergence factors in velocity formulation for both of the results in tables 3.1 and 3.3 are 0.56 with linear element and 0.76 with quadratic elements).

3.2. Weighted boundary functional. With the same reasoning that was suggested in section 3.1, we apply a different approach in this section to alleviate the trouble from corner points. Here, instead of strongly imposing boundary conditions in the solution space, we use weighted boundary functional to reduce the affect of corner points. This leads us to the following modified functionals:

$$F_{S_b} = F_S + \|\mathbf{u} - \mathbf{g}\|^2_{H^{\frac{1}{2}}(\partial\Omega)} + \|w(\mathbf{n} \times \mathbf{U} - \mathbf{G})\|^2_{H^{\frac{1}{2}}(\partial\Omega)}$$

and

$$G_{S_b} = G_S + \|\mathbf{u} - \mathbf{g}\|^2_{H^{\frac{1}{2}}(\partial\Omega)} + \|w(\mathbf{n} \cdot \mathbf{w} - g)\|^2_{H^{\frac{1}{2}}(\partial\Omega)},$$

where w is a smooth weight function defined by

$$w(r) = \begin{cases} r^{\beta}, & \text{if } r < \epsilon/2, \\ q(r), & \text{if } \epsilon/2 \le r \le \epsilon, \\ 1, & \text{if } r > \epsilon, \end{cases} \tag{3.5}$$

with r the distance from each corner, β a weighting parameter, and $q(r)$ an appropriately chosen polynomial. Throughout this paper, we use a $\mathcal{C}^2$-weight function, $w(r)$, satisfying (3.5) and defined by $w(r) = 1 + (r-\epsilon)^3(\eta^{-3}(1-\eta^{\beta}) + \eta^{-4}(3-(\beta+3)\eta^{\beta})(r-\eta) + \eta^{-5}(6-0.5(\beta^2+5\beta+12)\eta^{\beta})(r-\eta)^2)$ with $\eta = \epsilon/2$ when $\epsilon/2 \le r \le \epsilon$. For practicality, we use the following bound to replace of the boundary functional term defined above. For the finite element functions, u,

$$\|u\|^2_{H^{\frac{1}{2}}(\partial\Omega)} \le ch^{-1}\|u\|^2_{L^2(\partial\Omega)}.$$

Similar to using the redefined normal vector, F_{S_b} and G_{S_b} improve mass conservation (see table 3.4).

Velocity-Gradient			
	Linear ($h = 1/16$)	Quadratic (1/8)	Quartic (1/4)
mass loss	95 %	28 %	3%
functional value	5.311×10^{-3}	4.356×10^{-4}	1.929×10^{-5}
Vorticity			
mass loss	99.9%	81%	14%
functional value	2.417×10^{-4}	6.435×10^{-5}	6.687×10^{-6}

TABLE 3.4
Mass loss: Square tube, Weighted boundary functional ($\beta = 1, \epsilon = 0.3$)

Although weighted boundary functionals improve the mass conservation, they sometimes slow multigrid convergence. For example, AMG-convergence factors in velocity formulation in table 3.4 are 0.67 with linear elements and 0.83 with quadratic elements (compare with AMG-convergence factors in subsection 3.1). Better AMG algorithms may alleviate this difficulty.

For all of the computations below, we use a smoothly changing normal vector on the boundary. We now turn to a fundamentally different approach to substantially further improve mass conservation while maintaining multigrid efficiency.

3.3. FOSLS/FOSLL*. In this section, we attempt to further improve mass conservation by combining the techniques of FOSLS and FOSLL*. See [8] for more details about FOSLL*. The basic idea is to solve a FOSLL* system and then use the resulting approximate solution in a special FOSLS formulation to obtain an enhanced solution for certain variables.

Consider the following generic, linear, first-order system:

$$\mathcal{L}\mathbf{V} = \begin{bmatrix} \mathcal{L}_{11} & \mathcal{L}_{12} \\ \mathcal{L}_{21} & \mathcal{L}_{22} \end{bmatrix} \begin{bmatrix} \mathbf{V}_1 \\ \mathbf{V}_2 \end{bmatrix} = \begin{bmatrix} \mathbf{F}_1 \\ \mathbf{F}_2 \end{bmatrix} = \mathbf{F}. \tag{3.6}$$

The least-squares method solves (3.6) by minimizing the residual functional

$$\mathcal{G}(\mathbf{W}; \mathbf{F}) = \|\mathcal{L}\mathbf{W} - \mathbf{F}\|^2 = \|\mathcal{L}_{11}\mathbf{W}_1 + \mathcal{L}_{12}\mathbf{W}_2 - \mathbf{F}_1\|^2 + \|\mathcal{L}_{21}\mathbf{W}_1 + \mathcal{L}_{22}\mathbf{W}_2 - \mathbf{F}_2\|^2$$

on a Hilbert space $\mathbf{H} := H_1 \times H_2$, in the weak sense: find $\mathbf{V} \in \mathbf{H}$ satisfying

$$\langle \mathcal{L}\mathbf{V}, \mathcal{L}\mathbf{W} \rangle = \langle \mathbf{F}, \mathcal{L}\mathbf{W} \rangle, \quad \forall \mathbf{W} \in \mathbf{H}. \tag{3.7}$$

To help understand the structure of $\mathcal{L}$, consider Stokes equations. Since the analysis is easier if the system has the same number of unknowns as equations in FOSLS, we introduce slack variables and extend the velocity-gradient FOSLS formulation for Stokes equation to the following system:

$$\mathcal{L}_{vg}\mathbf{V} = \left[\begin{array}{cc|ccc} \nabla\times & -\nabla & I & \mathbf{0} & 0 \\ \nabla\cdot & \mathbf{0} & \mathbf{0} & \mathbf{0} & 0 \\ \hline \mathbf{0} & \mathbf{0} & \nabla\times & -\nabla & 0 \\ \mathbf{0} & \mathbf{0} & \nabla\cdot & \mathbf{0} & -\nabla \\ \mathbf{0} & \nabla\cdot & \mathbf{0} & \mathbf{0} & 0 \end{array}\right] \left[\begin{array}{c} \Phi \\ \mathbf{u} \\ \mathbf{U} \\ \phi \\ p \end{array}\right] = \left[\begin{array}{c} \mathbf{0} \\ 0 \\ \mathbf{0} \\ 0 \\ 0 \end{array}\right], \qquad (3.8)$$

where ϕ is a 3×1 vector of slack variables and Φ is a 3×3 matrix of slack variables with boundary conditions $\phi = \mathbf{0}$ and $\mathbf{n} \times \Phi = \mathbf{0}$ on $\partial\Omega$, respectively. Here, by letting $U_{33} = -U_{11} - U_{22}$ when $\mathbf{U} = \{U_{i,j}\}$, $i, j = 1, 2, 3$, we implicitly include the equation $\nabla(tr\mathbf{U}) = 0$. Again, $U_{33} = -U_{11} - U_{22}$ is imposed strongly in all numerical experiments to avoid the extra term $\|\nabla(tr\mathbf{U})\|$. In (3.8), we can define

$$\mathcal{L}_{11} = \left[\begin{array}{cc} \nabla\times & -\nabla \\ \nabla\cdot & \mathbf{0} \end{array}\right], \quad \mathcal{L}_{12} = \left[\begin{array}{ccc} I & \mathbf{0} & 0 \\ \mathbf{0} & \mathbf{0} & 0 \end{array}\right], \quad \mathcal{L}_{21} = \left[\begin{array}{cc} \mathbf{0} & \mathbf{0} \\ \mathbf{0} & \mathbf{0} \\ \mathbf{0} & \nabla\cdot \end{array}\right],$$

$$\text{and} \quad \mathcal{L}_{22} = \left[\begin{array}{ccc} \nabla\times & -\nabla & 0 \\ \nabla\cdot & \mathbf{0} & -\nabla \\ \mathbf{0} & \mathbf{0} & 0 \end{array}\right].$$

For the vorticity FOSLS, we use the formulation (2.3). Then, we have

$$\mathcal{L}_{vor}\mathbf{V} = \left[\begin{array}{cc|cc} \nabla\times & \nabla & -I & 0 \\ -\nabla\cdot & 0 & \mathbf{0} & 0 \\ \hline \mathbf{0} & \mathbf{0} & \nabla\times & \nabla \\ \mathbf{0} & \mathbf{0} & -\nabla\cdot & 0 \end{array}\right] \left[\begin{array}{c} \mathbf{u} \\ \alpha \\ \mathbf{w} \\ p \end{array}\right] = \left[\begin{array}{c} \mathbf{0} \\ 0 \\ \mathbf{0} \\ 0 \end{array}\right], \qquad (3.9)$$

where α is a scalar slack variable, and

$$\mathcal{L}_{11} = \left[\begin{array}{cc} \nabla\times & \nabla \\ -\nabla\cdot & 0 \end{array}\right], \quad \mathcal{L}_{12} = \left[\begin{array}{cc} -I & 0 \\ \mathbf{0} & 0 \end{array}\right], \quad \mathcal{L}_{21} = \left[\begin{array}{cc} \mathbf{0} & 0 \\ \mathbf{0} & 0 \end{array}\right], \quad \text{and } \mathcal{L}_{22} = \mathcal{L}_{11}.$$

If $\mathcal{L}$ is continuous and coercive, then the range of $\mathcal{L}$ is closed, which, in turn, implies that, if $\mathcal{L}\mathbf{V} = \mathbf{F}$ has a solution in $\mathbf{H}$, then $\mathcal{L}\mathcal{L}^*\tilde{\mathbf{V}} = \mathbf{F}$ has a solution in the domain of $\mathcal{L}^*$, which we denote by $\mathbf{S}$ (see lemma 2.1 in [8]). Thus, $\mathbf{V} = \mathcal{L}^*\tilde{\mathbf{V}}$ is the solution.

The FOSLL* approach directly addresses the system $\mathcal{L}^*\tilde{\mathbf{V}} = \mathbf{V}$. Here, the corresponding dual problem of (3.6) is

$$\mathcal{L}^*\tilde{\mathbf{V}} = \left[\begin{array}{cc} \mathcal{L}_{11}^* & \mathcal{L}_{21}^* \\ \mathcal{L}_{12}^* & \mathcal{L}_{22}^* \end{array}\right] \left[\begin{array}{c} \tilde{\mathbf{V}}_1 \\ \tilde{\mathbf{V}}_2 \end{array}\right] = \left[\begin{array}{c} \mathbf{V}_1 \\ \mathbf{V}_2 \end{array}\right]. \qquad (3.10)$$

The FOSLL* scheme minimizes the least-squares dual functional,

$$\mathcal{G}^*(\tilde{\mathbf{V}}; \mathbf{V}) = \|\mathcal{L}^*\tilde{\mathbf{V}} - \mathbf{V}\|^2,$$

on a Hilbert space, $\mathbf{S}$, and the corresponding weak formulation is: find $\tilde{\mathbf{V}} \in \mathbf{S}$ satisfying

$$\left\langle \mathcal{L}^*\tilde{\mathbf{V}}, \mathcal{L}^*\mathbf{Z} \right\rangle = \langle \mathbf{V}, \mathcal{L}^*\mathbf{Z} \rangle = \langle \mathbf{F}, \mathbf{Z} \rangle, \quad \forall \mathbf{Z} \in \mathbf{S}. \qquad (3.11)$$

Note that the right-hand side is computable. This may be viewed as a Galerkin approximation to $\mathcal{L}\mathcal{L}^*\tilde{\mathbf{V}} = \mathbf{F}$.

Now, we introduce a technique to obtain an enhanced approximation for variable $\mathbf{V}_1$ by FOSLL*. In the finite-dimensional subspace $\mathbf{S}^h \subset \mathbf{S}$, FOSLL* is approximately solved to get $(\tilde{\mathbf{V}}_1^h, \tilde{\mathbf{V}}_2^h) \in \mathbf{S}^h$. We then have

$$\left[\begin{array}{cc} \mathcal{L}_{11}^* & \mathcal{L}_{21}^* \\ \mathcal{L}_{12}^* & \mathcal{L}_{22}^* \end{array} \right] \left[\begin{array}{c} \tilde{\mathbf{V}}_1^h \\ \tilde{\mathbf{V}}_2^h \end{array} \right] = \left[\begin{array}{c} \mathbf{V}_1^h \\ \mathbf{V}_2^h \end{array} \right]. \tag{3.12}$$

Suppose that $\mathcal{L}_{11}$ is coercive and continuous on H$_1$ and that $\mathcal{L}_{12}$ does not contain any derivatives. Then, from the approximation obtained by FOSLL* in (3.12), we can get an enhanced approximate solution, $\mathbf{V}_1^h$, for $\mathbf{V}_1$ from the following system:

$$\mathcal{L}_{11}\mathbf{V}_1^h = \mathbf{F}_1 - \mathcal{L}_{12}\mathbf{V}_2^h = \mathbf{F}_1 - \mathcal{L}_{12}(\mathcal{L}_{12}^*\tilde{\mathbf{V}}_1^h + \mathcal{L}_{22}^*\tilde{\mathbf{V}}_2^h). \tag{3.13}$$

It is easy to see that, for $\mathbf{F}_1 = 0$,

$$\|\mathcal{L}_{11}(\mathbf{V}_1 - \mathbf{V}_1^h)\| = \|\mathcal{L}_{12}(\mathcal{L}_{12}^*(\tilde{\mathbf{V}}_1 - \tilde{\mathbf{V}}_1^h) + \mathcal{L}_{22}^*(\tilde{\mathbf{V}}_2 - \tilde{\mathbf{V}}_2^h))\|$$
$$\leq \|\mathcal{L}_{12}\| \, \|\mathbf{V}_2 - \mathbf{V}_2^h\|.$$

Thus, the enhanced approximation inherits the same order of convergence as the FOSLL* approximation.

Our aim is to use the FOSLS and FOSLL* schemes together to obtain better mass conservation. We rewrite the first-order systems of Stokes equations in the form

$$\mathcal{L}\mathbf{V} = \mathbf{F},$$

where $\mathbf{V} = (\Phi, \mathbf{u}, \mathbf{U}, \phi, p)^t$ in the velocity-gradient formulation, $\mathbf{V} = (\mathbf{u}, \alpha, \mathbf{w}, p)^t$ in the vorticity formulation, and $\mathcal{L}$ is the corresponding linear operator. The framework of FOSLS/FOSLL* approach follows. First, we obtain $\mathbf{V}_0^h$ by minimizing $\|\mathcal{L}\mathbf{V} - \mathbf{F}\|^2$ over an appropriate finite element space and then consider the residual equation,

$$\mathcal{L}\mathbf{W} = \mathbf{F} - \mathcal{L}\mathbf{V}_0^h \; (:= \mathbf{R}), \tag{3.14}$$

where $\mathbf{W} = \mathbf{V} - \mathbf{V}_0^h$. Next, we use the corresponding dual problem to get an L^2 approximation, $\mathbf{W}^h$, to $\mathbf{W}$. Since we solve for the differences with FOSLL*, this approach fits well for the Navier-Stokes equations. We discuss this in detail in section 4. We obtain $\mathbf{W}^h = \mathcal{L}^*\tilde{\mathbf{W}}^h$ by minimizing $\|\mathcal{L}^*\tilde{\mathbf{W}}^h - \mathbf{W}\|$ over an appropriate finite element space, which is computed using the weak form:

$$< \mathcal{L}^*\tilde{\mathbf{W}}^h, \mathcal{L}^*\tilde{\mathbf{Z}}^h > = < \mathbf{R}, \tilde{\mathbf{Z}}^h > .$$

We, then, construct the hybrid solution that combines the original H^1 approximation and the L^2 approximation,

$$\hat{\mathbf{V}}^h = \mathbf{V}_0^h + \mathbf{W}^h.$$

We call this a hybrid solution because, in general, $\mathbf{V}_0^h$ will be from an H^1 conforming finite element space, while $\mathbf{W}^h$ will be the image of an H^1 conforming finite element function under $\mathcal{L}^*$.

Finally, we obtain the enhanced approximation, $\mathbf{V}_1^h$, by minimizing the functional

$$\|\mathcal{L}_{11}\mathbf{V}_1^h + \mathcal{L}_{12}\hat{\mathbf{V}}_2^h - \mathbf{F}_1\|. \tag{3.15}$$

Velocity-Gradient		
	Linear ($h = 1/16$)	Quadratic ($1/8$)	Quartic ($1/4$)
mass loss	18%	0.16 %	0.03%

Vorticity		
mass loss	87%	35%	1.5%

TABLE 3.5

Mass loss: Square tube, FOSLS/FOSLL*-sn (smoothly changing normal)

The assumption that $\mathcal{L}_{12}$ contain no derivatives assures that $\mathcal{L}_{12}\hat{\mathbf{V}}_2^h \in L^2$.

In the context of the velocity-gradient form of Stokes equations, the process is simplified because of the slack variables. From (3.8), setting the slack variable $\Phi = 0$ reduces (3.15) to the minimization $\|\nabla\mathbf{u} - \hat{\mathbf{U}}^h\|$. Here, the hybrid approximation, $\hat{\mathbf{U}}^h$, is obtained through the process described above. To be more precise, $\hat{\mathbf{U}}^h = \mathbf{U}_0^h + \mathbf{U}_1^h$, where $\mathbf{U}_0^h$ comes from the H^1 minimization and $\mathbf{U}_1^h$ comes from the L^2 minimization of the residual equation as part of $\mathcal{L}_{12}^*\,\tilde{\mathbf{W}}_1^h + \mathcal{L}_{22}^*\,\tilde{\mathbf{W}}_2^h$, namely

$$\mathbf{U}_1^h := \tilde{\Phi}^h + \nabla \times \tilde{\mathbf{U}}^h - \nabla\tilde{\phi}^h,$$

where $\tilde{\mathbf{W}}_1^h = (\tilde{\Phi}^h, \tilde{\mathbf{u}}^h)^t$ and $\tilde{\mathbf{W}}_2^h = (\tilde{\mathbf{U}}^h, \tilde{\phi}^h, \tilde{p}^h)^t$.

Finally, we get an enhanced approximation for $\mathbf{u}$ by minimizing

$$\mathcal{G}_{vg}(\mathbf{u}; \hat{\mathbf{U}}^h) = \|\nabla\mathbf{u} - \hat{\mathbf{U}}^h\|^2 + \|\nabla \cdot \mathbf{u}\|^2,$$

again over an appropriate finite element space.

Analogously for the vorticity FOSLS formulation, we form a hybrid approximation, $\hat{\mathbf{w}}^h = \mathbf{w}_0^h + \mathbf{w}_1^h$, where $\mathbf{w}_0^h$ comes from the H^1 minimization and $\mathbf{w}_1^h$ comes from the L^2 minimization on the residual equations as part of $\mathcal{L}^*\tilde{\mathbf{W}}^h$, namely

$$\mathbf{w}_1^h := -\tilde{\mathbf{u}}^h + \nabla \times \tilde{\mathbf{w}}^h + \nabla\tilde{P}^h.$$

We obtain an enhanced approximation of $\mathbf{u}$ by minimizing the functional
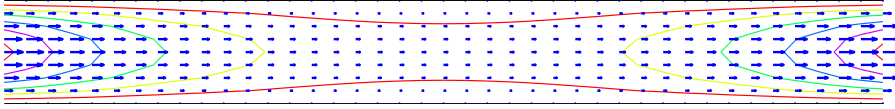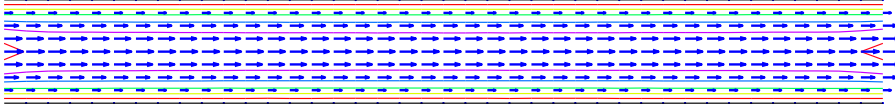
$$\mathcal{G}_{vor}(\mathbf{u}; \hat{\mathbf{w}}^h) = \|\nabla \times \mathbf{u} - \hat{\mathbf{w}}^h\|^2 + \|\nabla \cdot \mathbf{u}\|^2,$$

where $\mathbf{w}^h = \mathbf{w}_0^h + \mathbf{w}_D^h$ is a hybrid approximation.

By applying the FOSLS/FOSLL* approach to (3.8) and (3.9), we obtain dramatically improved mass conservations. In the velocity-gradient formulation, the method of FOSLS/FOSLL* reduces the mass loss from 76.2% to 0.16% with quadratic finite elements and mesh $h = 1/8$ on the $1 \times 1 \times 10$ domain (see table 3.5 and compare to tables 3.3 and 3.4). (For these computations, we use a smoothly changing normal vector on the boundary in both of FOSLS and FOSLL* steps in FOSLS/FOSLL*.)

Also, we compare FOSLS and FOSLS/FOSLL* in terms of the central cross-section of flow through the domain in figures 3.5 and 3.6, respectively, where the lines are contour lines of the flow and the arrows are the flow field. The flow dissipates when only FOSLS is used. As figure 3.6 shows, with FOSLS/FOSLL*, the parabolic profile at the inlet immediately changes to steady flow, which means that it is essentially independent of z-direction, until right before it reaches the outlet where the parabola boundary condition is specified.

To explain why the FOSLS/FOSLL* approach improves mass conservation, consider the following simple example. Assume that we have a linear first-order system, $\mathcal{L}U = F$, where $\|\mathcal{L}U\|^2$ is equivalent to the H^1-seminorm, $|U|_{H^1(\Omega)}^2 = \|\nabla U\|^2$. Here,

FIG. 3.5. *Cross section of flow with standard velocity FOSLS (quadratic elements, $h = 1/8$)*

FIG. 3.6. *Cross section of flow with velocity FOSLS/FOSLL*-sn (quadratic elements, $h = 1/8$)*

coercivity in the H^1 norm is established through a Poincaré-type inequality. First, by minimizing $\|\mathcal{L}U - F\|^2$, we obtain an approximate solution, U_0^h, in a finite element space, $\mathbf{H}^h$. That is, U_0^h is the minimizer of the functional $\|\mathcal{L}V^h - F\|^2$, which is equivalent to $|V^h - U|^2_{H^1(\Omega)}$, in the finite-dimensional space $\mathbf{H}^h$. While FOSLS minimizes the error in H^1-seminorm, FOSLL* minimizes the error in L^2-norm by minimizing $\|\mathcal{L}^*\tilde{D} - D\|^2$, which is equivalent to $\|D^h - D\|^2$, where $D^h = \mathcal{L}^*\tilde{D}$ and $D = U - U_0^h$. Then, our hybrid approximation for U is $U^h = U_0^h + D^h$. This new approximate solution is composed of our best approximate solution, U_0^h, in a current least-squares finite element space (H^1-conforming space) obtained from minimizing the error in an H^1-seminorm-equivalent functional and a correction, D^h, that is obtained by minimizing an L^2-equivalent functional. The correction D^h is the image of an H^1-conforming finite element function under $\mathcal{L}^*$. In essence, D^h is from an L^2-conforming space, and will, in general, be discontinuous.

3.4. Backward-facing step. Consider the backward-facing step domain shown in figure 3.7. An analysis of the least-squares method for Navier-Stokes equations on such a domain can be found in [11]. Our prototype domain has the ratio $1 \times 1 \times 10$ and the step has a height 0.5 and a length 2, that is, a $1 \times 0.5 \times 2$ notch of the bottom corner is removed. The velocity boundary condition on the outlet ($z = 10$) is the same
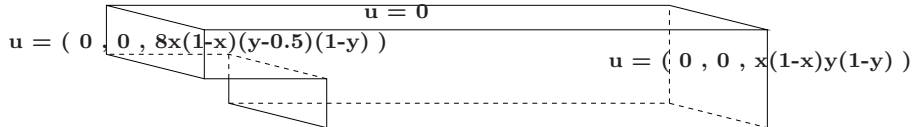

FIG. 3.7. *Backward facing step domain*

as given in (3.1) and the velocity boundary condition on the inlet ($z = 0, y > 0.5$) is given by

$$\mathbf{n} \times \mathbf{u} = \mathbf{0} \quad \text{and} \quad \mathbf{n} \cdot \mathbf{u} = 8x(1 - x)(y - 0.5)(1 - y). \tag{3.16}$$

A no-slip boundary condition is imposed along the walls. The domain has a reentrant edge, which means an edge with the inner angle bigger than π, where $y = 0.5$ and $z = 2$. Therefore, F_S is not equivalent to the H^1-norm because of the singularity on the boundary and this singularity may result in a loss of global accuracy. Weight functions can be used around the singularity to overcome this difficulty [13],[14]. Here, we use a typical weight function, $w(r)$, defined as in (3.5), where r is now the distance from the reentrant edge and ϵ is the radius of the weight function, with $\beta = 2$ and

radius $\epsilon = 0.3$ used in our numerical experiments in this section. The aim, now, is to minimize the functionals

$$F_{S_w}(\mathbf{u}, \mathbf{U}, p) = \|\mathbf{U} - \nabla\mathbf{u}\|^2 + \|\nabla \cdot \mathbf{u}\|^2$$
$$+ \|\nabla \cdot \mathbf{U} - \nabla p\|_w^2 + \|\nabla \times \mathbf{U}\|_w^2 + \|\nabla(tr\mathbf{U})\|_w^2 \qquad (3.17)$$

and

$$G_{S_w}(\mathbf{u}, \alpha, \mathbf{w}, p) = \|\nabla\times\mathbf{u} +\nabla\alpha -\mathbf{w}\|^2 + \|\nabla \cdot \mathbf{u}\|^2 + \|\nabla\times\mathbf{w} +\nabla p\|_w^2 + \|\nabla \cdot \mathbf{w}\|_w^2, \qquad (3.18)$$

where $\|\cdot\|_w^2 = \int_\Omega w(r)^2 |\cdot|^2 d\Omega$. Note that we do not use any mesh refinement around the singularity as this will not alleviate the difficulty.

The observation suggests that most of the mass loss occurs near $z = 2$ where the narrow tube becomes enlarged. Table 3.6 compares the results with standard FOSLS, FOSLS-sn (smoothly changing normal vector), and FOSLS/FOSLL* when quadratic elements on mesh $h = 1/8$ are used in the velocity-gradient formulation. Figures 3.8 and 3.9 show cross-sections of the flow, $\mathbf{u}$, at $x = 0.5$. If we use quartic elements with $h = 1/4$ for F_{S_w}, then the mass loss reduces to 61% (functional=1.222×10^{-2}) for standard FOSLS and 15% (functional=1.708×10^{-3}) for FOSLS with a smoothly changing normal vector.

	FOSLS	FOSLS-sn	FOSLS/FOSLL*-sn
mass loss	86 %	33%	3%

Table 3.6
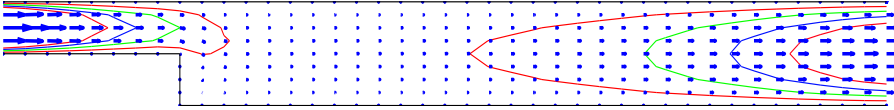*Mass loss: Backward step, Stokes velocity-gradient, Quadratic elements, Mesh $h = 1/8$*

Fig. 3.8. *Cross-section of flow with standard velocity FOSLS (quadratic elements, $h = 1/8$)*
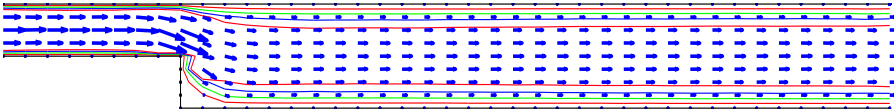

Fig. 3.9. *Cross-section of flow with velocity FOSLS/FOSLL* (quadratic elements, $h = 1/8$)*

Table 3.7 shows the mass loss from minimizing the vorticity FOSLS functional (3.18) with and without modification of the normal vectors. Compare the results with smoothly changing normal vector and quadratic elements with mesh $h = 1/8$ for the velocity-gradient formulation (table 3.6) and the vorticity formulation (table 3.7). The former shows a mass loss of 33% while the latter suffers a mass loss of 81%. In the case of a domain with a reentrant edge, the vorticity formulation shows a greater mass loss. We see similar behavior with Navier-Stokes equations and will explain more details in the following section.

4. Mass conservation for the Navier-Stokes equations. In this section, we return our attention to the Navier-Stokes equations introduced in section 2. All of the approaches suggested in section 3 can be easily applied to the Navier-Stokes equations. For example, if we use a smoothly changing normal vector in the square

	Linear(h=1/16)	Quadratic(1/8)	Quartic(1/4)
FOSLS	99.99%	99.99%	99.99%
functional value	1.182×10^{-2}	4.292×10^{-3}	2.295×10^{-3}
FOSLS-sn	99.9 %	81%	24%
functional value	1.064×10^{-2}	2.108×10^{-3}	4.238×10^{-4}

TABLE 3.7
Mass loss: Backward step, Stokes vorticity, FOSLS and FOSLS-sn

tube $(1 \times 1 \times 10)$, then we can reduce the loss of mass in the middle of domain from 76% to 16.6% with quadratic elements and $h = 1/8$ for $Re = 100$ by using the velocity-gradient formulation (2.4).

It is known that scaling often helps the mass conservation for large Re ([10]). We, thus, consider the Navier-Stokes functional rescaled by $\sqrt{Re}$ [10]:

$$F_{N_w}(\mathbf{u}, \mathbf{U}, p : \mathbf{0}) = \|\mathbf{U} - \nabla\mathbf{u}\|^2 + \|\nabla \cdot \mathbf{u}\|^2 + \| -\sqrt{Re}\mathbf{u} \cdot \mathbf{U} - \frac{1}{\sqrt{Re}}\nabla p + \frac{1}{\sqrt{Re}}\nabla \cdot \mathbf{U}\|_w^2$$

$$+ \|\frac{1}{\sqrt{Re}}\nabla \times \mathbf{U}\|_w^2 + \|\nabla(tr\mathbf{U})\|_w^2, \tag{4.1}$$

where $\| \cdot \|_w^2 = \int_\Omega w^2| \cdot |^2 d\Omega$, $w = 1$ in a regular domain, and $w = w(r)$ defined as in (3.5) in the presence of a reentrant edge with r the distance from the reentrant edge. In table 4.1, we compare the numerical results with and without scaling in the functional in the square tube.

minimizing functional	FOSLS	FOSLS-sn
(2.4) F	76%	16.6%
(4.1) F_{N_w} $(w = 1)$	11%	2.6%

TABLE 4.1
Mass loss: Square tube, Navier-Stokes velocity-grad, $Re = 100$, Quadratic elements, Mesh $h = 1/8$

Dividing the third and fourth terms on the right side in (2.4) by $\sqrt{Re}$ emphasizes the first, second, and fifth equations in the least-squares minimization. Thus, mass is better preserved because of the increased emphasis on the mass equation, $\nabla \cdot \mathbf{u} = 0$, in minimization. (Recall that the trace constraint is enforced by eliminating one dependent variable.) For example, when $Re = 500$, mass loss is reduced to 1.2% with the functional (4.1), smoothly changing normal vector, quadratic elements, and $h = 1/8$. Fortunately, adding a scalar weight to these equations can have a positive effect on the performance of solvers. In general, we find that (4.1) yields better AMG performance. For instance, in the tests described in table 4.1, the AMG convergence factors were 0.81 with the original functional (2.4) and 0.62 with the rescaled functional (4.1).

Next, we focus on the FOSLS/FOSLL* approach introduced in section 3.3, which is perhaps more compelling for the nonlinear Navier-Stokes equations because applying FOSLL* amount to just one more linearization in the framework of Newton iterations. We first apply Newton's method to the first-order nonlinear systems (2.2) and (2.3), or their rescaled versions, and then approximately solve the resulting linearized problem as follows. Systems (2.2) and (2.3), or their rescaled versions can be written in the form

$$\mathcal{L}(\mathbf{V}) = \mathbf{0}, \tag{4.2}$$

where $\mathcal{L}$ is a corresponding nonlinear operator. We linearize (4.2) around $\mathbf{V}_0$ by applying Newton's method:

$$\mathcal{L}'(\mathbf{V}_0)[\ \mathbf{V} - \mathbf{V}_0] = -\mathcal{L}(\mathbf{V}_0), \tag{4.3}$$

where $\mathcal{L}'(\mathbf{V}_0)[\mathbf{V} - \mathbf{V}_0]$ denotes the first Fréchet derivative of $\mathcal{L}$ at $\mathbf{V}_0$ in direction $\mathbf{V} - \mathbf{V}_0$. By letting $\hat{\mathcal{L}} = \mathcal{L}'(\mathbf{V}_0)$, $\mathbf{W} = \mathbf{V} - \mathbf{V}_0$, and $\mathbf{F} = -\mathcal{L}(\mathbf{V}_0)$, we recast (4.3) as

$$\hat{\mathcal{L}}\mathbf{W} = \mathbf{F}. \tag{4.4}$$

We then apply the least-squares method, that is, we minimize the residual functional

$$\|\hat{\mathcal{L}}\mathbf{W} - \mathbf{F}\|^2.$$

Once we have an approximation, $\mathbf{W}^h$, for $\mathbf{W}$, then our new approximation for $\mathbf{V}$ is $\mathbf{V}_0 + \mathbf{W}^h$. This is one Newton iteration in a least-squares context. After doing a sufficient number of Newton iterations, we then do one final linearization and again consider linear system (4.4). Now, however, instead of minimizing the functional $\|\hat{\mathcal{L}}\mathbf{W} - \mathbf{F}\|$, we solve for the dual problem $\hat{\mathcal{L}}^*\tilde{\mathbf{W}} = \mathbf{W}$ to get a hybrid approximation to $\mathbf{V}$ and an enhanced approximation to the velocity, $\mathbf{u}$, in accordance with the FOSLS/FOSLL* approach. We obtain an approximation $\mathbf{W}^h$ ($:= \hat{\mathcal{L}}^*\tilde{\mathbf{W}}^h$) of $\mathbf{V} - \mathbf{V}_0$ by solving the corresponding variational formulation of the dual minimization problem: find $\tilde{\mathbf{W}}$ satisfying

$$\tilde{\mathbf{W}} = arg\ \min_{\tilde{\mathbf{Z}}} \|\hat{\mathcal{L}}^*\tilde{\mathbf{Z}} - \mathbf{W}\|.$$

Our hybrid approximation for $\mathbf{V}$ is thus $\mathbf{V}^h = \mathbf{V}_0 + \mathbf{W}^h$ and we then get the enhanced approximation of the velocity by minimizing the FOSLS functional

$$\|\nabla\mathbf{u} - \mathbf{U}^h\|^2 + \|\nabla \cdot \mathbf{u}\|^2 \quad \text{or} \quad \|\nabla \times \mathbf{u} - \mathbf{w}^h\|^2 + \|\nabla \cdot \mathbf{u}\|^2, \tag{4.5}$$

where $\mathbf{U}^h$ and $\mathbf{w}^h$ are elements of the hybrid approximation, $\mathbf{V}^h = \mathbf{V}_0 + \hat{\mathcal{L}}^*\tilde{\mathbf{W}}^h$.

In the following subsections, we compare the methods described above for Navier-Stokes equations in the backward facing step domain. Since there is a singular edge on the boundary, we redefine the functionals in (2.4) and (2.5) to
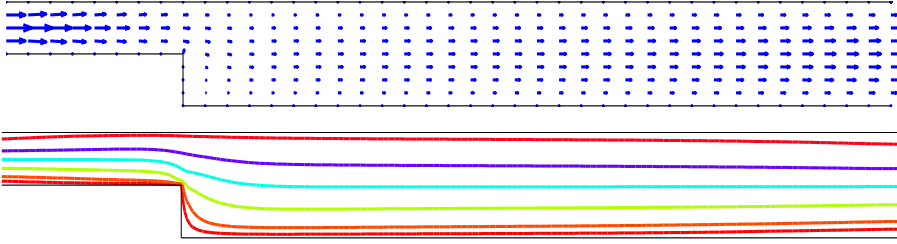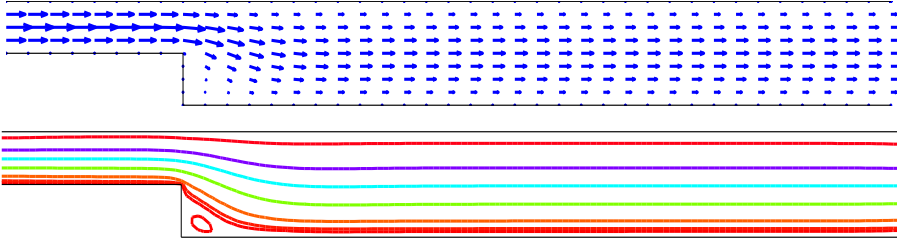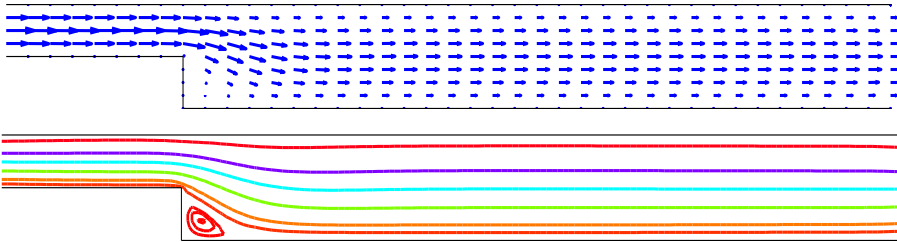
$$\begin{aligned} F_w(\mathbf{u}, \mathbf{U}, p : \mathbf{0}) = \ &\|\mathbf{U} - \nabla\mathbf{u}\|^2 + \|\nabla \cdot \mathbf{u}\|^2 \\ &+ \| - Re\mathbf{u} \cdot \mathbf{U} - \nabla p + \nabla \cdot \mathbf{U}\|_w^2 + \|\nabla \times \mathbf{U}\|_w^2 + \|\nabla(tr\mathbf{U})\|_w^2 \end{aligned} \tag{4.6}$$

and

$$\begin{aligned} G_w(\mathbf{u}, \alpha, \mathbf{w}, P : \mathbf{0}) = \ &\|\nabla \times \mathbf{u} + \nabla\alpha - \mathbf{w}\|^2 + \|\nabla \cdot \mathbf{u}\|^2 \\ &+ \| - Re\mathbf{u} \times \mathbf{w} + \nabla P + \nabla \times \mathbf{w}\|_w^2 + \|\nabla \cdot \mathbf{w}\|_w^2, \end{aligned} \tag{4.7}$$

respectively, where $\|\cdot\|_w$ is a weighted norm defined as in (4.1).

4.1. Backward-facing step: velocity-gradient FOSLS formulation. In this subsection, Navier-Stokes in a backward-facing step domain is considered. The domain is the same as shown in figure 3.7. All of the numerical results in this subsection are based on minimization of the velocity-gradient formulation least-squares functional with quadratic elements and $h = 1/8$. Here, we set the weight parameter $\beta = 2$ and radius $\epsilon = 0.125$ in (3.5) and use the corresponding weighted-norm

FIG. 4.1. *Velocity flow and stream lines with standard FOSLS at $x = 0.5$, $Re = 500$*

FIG. 4.2. *Velocity flow and stream lines with rescaled sm-FOSLS at $x = 0.5$, $Re = 500$*

FIG. 4.3. *Velocity flow and stream lines with rescaled sm-FOSLS/FOSLL* at $x = 0.5$, $Re = 500$*

for the third and fourth terms in (2.4) and (4.1). By letting $U_{33} = -U_{11} - U_{22}$ where $\mathbf{U} = \{U_{i,j}\}$, $i, j = 1, 2, 3$, the equation $\nabla(tr\mathbf{U}) = 0$ is included implicitly. We compare numerical results with the Reynolds number $Re = 100$ and 500. The most mass loss occurs where the flow enters the bigger channel at $z = 2$. As briefly mentioned at the beginning of section 4, table 4.2 shows that in rescaled functional the larger Reynolds number provides better mass conservation. Similarly to Stokes case, a smoothly changing normal vector and the correction from FOSLS/FOSLL* both improve mass conservation.

	functional	FOSLS	FOSLS-sn	FOSLS/FOSLL*-sn
$Re = 100$	(4.6) F_w	92%	73%	43.7%
	(4.1) F_{N_w}	35%	25%	8%
$Re = 500$	(4.6) F_w	87%	56%	0.6%
	(4.1) F_{N_w}	13%	10%	0.2%

TABLE 4.2
Mass loss : Backward step, Navier-Stokes velocity-grad, Quadratic elements, $h = 1/8$

In figures 4.1, 4.2, and 4.3, we compare the cross sections of velocity flows and stream lines with different approaches when the Reynolds number is 500. The velocity flow and steam line in figure 4.1 are obtained by minimizing the standard FOSLS functional (2.4) with no modification in normal vector. Figure 4.2 is from the mini-

mization of the rescaled functional (4.1) with a smoothly changing normal vector and figure 4.3 is after replacing FOSLS with FOSLL* after the last Newton iteration of the result in figure 4.2. In figure 4.2, the recirculation at the left bottom starts to appear and this recirculation appears more clearly in figure 4.3 while the standard FOSLS approach does not show any recirculation.

4.2. Backward-facing step: vorticity FOSLS formulation. We now consider the vorticity functional (2.5) and following rescaled functional in a partially weighted norm with $Re = 100$ and 500:

$$G_{N_w}(\mathbf{u}, \alpha, \mathbf{w}, P : \mathbf{0}) = \|\nabla \times \mathbf{u} + \nabla\alpha - \mathbf{w}\|^2 + \|\nabla \cdot \mathbf{u}\|^2$$
$$+\| -\sqrt{Re}\mathbf{u} \times \mathbf{w} + \frac{1}{\sqrt{Re}}\nabla P + \frac{1}{\sqrt{Re}}\nabla \times \mathbf{w}\|_w^2 + \|\frac{1}{\sqrt{Re}}\nabla \cdot \mathbf{w}\|_w^2. \quad (4.8)$$

We use the $1 \times 1 \times 7$ tube with a $1 \times 0.5 \times 2$ notch in the lower left corner removed. Again, we set the weight parameter $\beta = 2$ and radius $\epsilon = 0.125$ in (3.5).

	functional	FOSLS	FOSLS-sn	FOSLS/FOSLL*-sn
$Re = 100$	(4.7) G_w	99.99 %	91%	92.4%
	(4.8) G_{N_w}	42.8%	35.6%	40%
$Re = 500$	(4.7) G_w	99.99%	97%	97.4%
	(4.8) G_{N_w}	51.3%	51%	56%

TABLE 4.3
Mass loss: Backward step, Navier-Stokes vorticity, Quadratic elements, $h = 1/8$

	functional	FOSLS	FOSLS-sn	FOSLS/FOSLL*-sn
$Re = 100$	(4.7) G_w	97%	43.6%	48%
	(4.8) G_{N_w}	13.4%	6.5%	9%
$Re = 500$	(4.7) G_w	97.5 %	61 %	69%
	(4.8) G_{N_w}	7.4%	6.7%	8.2%

TABLE 4.4
Mass loss: Backward step, Navier-Stokes vorticity, Quartic elements, $h = 1/4$

Tables 4.3 and 4.4 show the mass loss with quadratic ($h = 1/8$) and quartic ($h = 1/4$) elements, respectively. Similarly to the results for the Stokes vorticity formulation in section 3.4, standard FOSLS formulation provides poor mass conservation. However, the rescaled functional improves mass conservation with higher-order elements.

The results in table 4.3 may lead us to the conclusion that the correction from FOSLL* does not improve mass conservation if the FOSLS solution is not good enough. However, table 4.4 shows that, with the vorticity formulation and in the presence of a reentrant edge, the FOSLL* step does not help mass conservation even though we have better mass-conserved approximate solution. For example, rescaled FOSLS with smoothly changing normal vector has 6.5% of mass loss with quartic elements and $h = 1/4$, but, after replacing the last Newton iteration with a FOSLL* hybrid solution, the mass loss is 9% which is a little bit worse than without the FOSLL* correction. Comparison with the results in table 3.5 from the square tube domain confirms that the singularity on the edge degrades the performance of FOSLS/FOSLL* approach in the vorticity formulation. Currently, we only have a rough guess of the reason for this. In the presence of a boundary singularity, which requires the use of a weight function, the div/curl system (in our case, the one induced from the vorticity FOSLS formulation) usually has trouble finding an accurate approximate solution

with H^1-conforming finite elements. Our guess is that the FOSLL*-step with div/curl system and boundary singularity may introduce more error in L^2-correction process in the context of a Newton iteration. Finding the exact reasons for failing to improve the mass conservation in vorticity formulation with the FOSLS/FOSLL* approach will be our future work.

In papers [9] and [10], we developed ways to enhance conservation in the vorticity formulation by introducing new variables.

5. Conclusion. Least-squares finite element methods minimize the continuity equation in an L^2-norm as one of a number of terms and, thus, do not enforce exact mass conservation in the solution space. In some contexts, this yields severe mass loss in the velocity flow, especially on under-resolved grids in long thin domains with velocity boundary conditions. In this paper, we introduce a modified normal vector near corners, a weighted-norm boundary functional, and a FOSLS/FOSLL* hybrid solution to reduce the loss of mass in both velocity-gradient and vorticity FOSLS formulations. Overall, results show that the velocity-gradient formulation conserves mass better than the vorticity formulation. Using a modified normal vector and weighted-norm boundary functional provide similar mass conservation, but the boundary functional approach often degrades the performance of the AMG solver while the modified normal vector does not affect the AMG solver. The best mass conservation is achieved by, in addition, forming a hybrid approximate solution using a FOSLL* correction in the velocity-gradient formulation with high-order elements. While the FOSLL* step involves extra work in the context of Stokes equations, it is just one of perhaps many Newton steps when solving the Navier-Stokes equations. Finally, we find that the FOSLS/FOSLL* approach does not help mass conservation in the vorticity formulation in the presence of a singularity. The explanation of this phenomena is the focus of future reserch.

REFERENCES

[1] P. Bochev, Z. Cai, T. A. Manteuffel, and S. F. McCormick, *Analysis of velocity-flux first-order system least-squares principles for the Navier-Stokes equations. I*, SIAM J. Numer. Anal., 35 (1998), pp. 990–1009.

[2] Pavel B. Bochev, *Analysis of least-squares finite element methods for the Navier-Stokes equations*, SIAM J. Numer. Anal., 34 (1997), pp. 1817–1844.

[3] Pavel B. Bochev and Max D. Gunzburger, *Analysis of least squares finite element methods for the Stokes equations*, Math. Comp., 63 (1994), pp. 479–506.

[4] ———, *Finite element methods of least-squares type*, SIAM Rev., 40 (1998), pp. 789–837.

[5] Z. Cai, R. Lazarov, T. A. Manteuffel, and S. F. McCormick, *First-order system least squares for second-order partial differential equations. I*, SIAM J. Numer. Anal., 31 (1994), pp. 1785–1799.

[6] Zhiqiang Cai, Thomas A. Manteuffel, and Stephen F. McCormick, *First-order system least squares for second-order partial differential equations. II*, SIAM J. Numer. Anal., 34 (1997), pp. 425–454.

[7] Z. Cai, T. A. Manteuffel, and S. F. McCormick, *First-order system least squares for the Stokes equations, with application to linear elasticity*, SIAM J. Numer. Anal., 34 (1997), pp. 1727–1741.

[8] Z. Cai, T. A. Manteuffel, S. F. McCormick, and J. Ruge, *First-order system $\mathcal{LL}^*$ (FOSLL*): scalar elliptic partial differential equations*, SIAM J. Numer. Anal., 39 (2001), pp. 1418–1445.

[9] J. J. Heys, E. Lee, T. A. Manteuffel, and S. F. McCormick, *On mass-conserving least-squares methods*, SIAM J. Sci. Comput., 28 (2006), pp. 1675–1693.

[10] ———, *An alternative least-squares formulation of the Navier-Stokes equations with improved mass conservation*, J. Comput. Phys., 226 (2007), pp. 994–1006.

[11] Bo-nan Jiang, *The least-squares finite element method*, Scientific Computation, Springer-

Verlag, Berlin, 1998. Theory and applications in computational fluid dynamics and electromagnetics.

[12] Bo-Nan Jiang and C. L. Chang, *Least-squares finite elements for the Stokes problem*, Comput. Methods Appl. Mech. Engrg., 78 (1990), pp. 297–311.

[13] E. Lee, T. A. Manteuffel, and C. R. Westphal, *Weighted-norm first-order system least squares (FOSLS) for problems with corner singularities*, SIAM J. Numer. Anal., 44 (2006), pp. 1974–1996.

[14] ———, *Weighted-norm first-order system least-squares (fosls) for div/curl systems with three dimensional edge singularities*, SIAM J. Numer. Anal., 46 (2008), pp. 1619–1639.

[15] J. P. Pontaza and J. N. Reddy, *Space-time coupled spectral/hp least-squares finite element formulation for the incompressible Navier-Stokes equations*, J. Comput. Phys., 197 (2004), pp. 418–459.

[16] John Ruge, *Fospack : A first-order system least-squares(fosls) code*, in preparation.

[17] Grit Thürmer and Charles Wüthrich, *Computing vertex normals from polygonal facets*, Journal of Graphics Tools, 3 (1998), pp. 43–46.